文章编号:1672-3961(2009)05-0001-20

Relaxation in glasses far from equilibrium

YUE Yuan-zheng[1,2]

(1. Section of Chemistry, Aalborg University, DK-9000 Aalborg, Denmark;
2. Key Laboratory of Liquid Structure and Heredity of Materials, Shandong University, Jinan 250061, China)

Abstract: This paper describes recent advances in the study of relaxation in hyperquenched glasses (HQGs), i.e., glasses far from equilibrium. The new approaches for determination of the fictive temperature and the cooling rate of the HQGs are introduced and two examples are presented. The hyperquenching-annealing-calorimetric scan (HAC) strategy is used to explore the energetic and structural heterogeneities in glasses. The occurrence of a pre-endotherm is observed when a properly annealed HQG undergoes a calorimetric upscan. The pre-endotherm is followed by an exotherm due to the release of the excess energy stored during hyperquenching, and subsequently by the endothermic glass transition. Several striking features of the pre-endotherm are demonstrated and compared with those of the glass transition. This comparison is crucial for understanding the non-linearity and non-exponentiality of the relaxation in glass. The data obtained from the HAC experiments on silicate glasses are used to clarify the glass transition of water. Fundamental differences in relaxation behavior between a strong and a fragile HQG are found and analyzed in terms of their structural and energetic origins. The strong impact of the annealing degree on the vibrational density of states of HQGs are exhibited and discussed in terms of microstructure.

Key words: glass; relaxation; hyperquenching; annealing; calorimetry; heat capacity; Boson peak

远离平衡态玻璃的弛豫

岳远征[1,2]

(1. 丹麦奥尔堡大学化学系, 丹麦, 奥尔堡 DK-9000;
2. 山东大学教育部材料液态结构及其遗传性重点实验室, 山东 济南 250061)

摘要:本文阐述了关于远离平衡态玻璃(即急冷玻璃)弛豫的最新研究进展.结合实例,介绍了测量及计算急冷玻璃假想温度和冷却速度的新途径.急冷－退火－热扫描的方法是探索玻璃中能量和结构非均匀性的理想手段.如果对一个适当退火的急冷玻璃升温差热扫描,将会先后出现预吸热峰,释放急冷中储存在玻璃中能量的放热峰,以及玻璃转变吸热峰.介绍和分析了预吸热峰的几个典型特征,并与玻璃转变吸热峰的特征进行比较,这对理解玻璃弛豫的非指数和非线性特征是极其关键的.用急冷－退火－热扫描方法在硅酸盐玻璃获得的数据,可在一定程度上揭示水的玻璃转变现象.急冷强玻璃和弱玻璃在弛豫行为上体现出本质差别,本文对其差别的结构和能量根源进行了讨论.退火度对急冷玻璃的振动态密度具有明显影响,并通过显微结构因素对这一影响进行了分析.

关键词:玻璃;弛豫;急冷;退火;热容;预吸热峰;震动态密度
中图分类号:TG146.4 **文献标志码**:A

1 Introduction

When a liquid is 'rapidly' cooled, it will bypass crystallization, get supercooled, and subsequently undergo a sudden drop in isobaric heat capacity (C_p) at some temperature. The extent of the sudden drop depends on the chemical composition. How "rapidly" the system should

Received date: 2009-05-06
Foundation item: This work was supported by Rockwool International A/S, and Danish Research Council for financial support under Grant No. 26-03-0096 and No. 274-07-0493.
Biography: YUE Yuan-zheng(1958-), male, Ph.D., Professor, his research deals with amorphous materials science. E-mail: yy@bio.aau.dk

be cooled to form a glass depends on the chemical nature of liquids. The sudden drop in C_p is due to the glass transition, i.e., the kinetic transition from liquid to glass. The temperature, at which the sudden drop occurs, is defined as the glass transition temperature (T_g), at which the structural relaxation takes about 30-100 seconds for most of glass formers[1]. When the system is further cooled, the structural relaxation will become so slow that it is undetectable within laboratory time scales. We then say that the system becomes a glass that, mechanically, behaves like a solid. Beside the conventional inorganic glasses, there are a large number of other types of glasses such as polymer glasses, proteins, spin glasses, and amorphous alloys. Glasses can also be obtained naturally, e.g., glasses formed during eruption of volcanoes. Recently, it is recognized that most of the universe's water exists in the glassy state.

It is known that, besides melt cooling, many other routes may also be applied to obtain a glass state[1]. For instance, vitreous silica can be prepared using different approaches such as vapor condensation, sol-gel technique, argon plasma, heavy particle bombardment of crystalline form. Very recently, it has been found that high purity mesoporous silica glass can be synthesized in aqueous solution under ambient conditions via biological catalysis[2]. However, the most important and frequently used route for glass forming is still the cooling or quenching of a liquid. Just in this simple process, a kinetic event, i.e., the glass transition occurs, which has puzzled scientists for many decades. Although substantial progress has been made in studying the glass transition, numerous key questions still remain unanswered. Just as the Nobel Laureate P.W. Anderson stated in 1995, the deepest and most important unsolved problem in condensed matter science is probably the theory of the nature of glass and the glass transition[3]. From the point of view of the present author, this statement still holds even for today, since many crucial questions remain unanswered[4-5]. This situation motivates scientists to continue to explore the glass transition.

Over the past decade, the research group of the present author has made considerable efforts to study the relaxation phenomena in glass and their impact on the glass transition. The study has been carried out using the hyperquenching-annealing-calorimetric scan (HAC) approach well described in [6-9]. Using the HAC approach, liquids can be arrested in unusually "excited" (high potential energy) states by hyperquenching (HQ) ($>10^3$ K·s^{-1}) due to the intrinsic slowing down of relaxation with a sudden drop of temperature. After such trapping at high "fictive" temperatures, we observe structural and energetic properties as the system evolves at low temperatures, during a controlled annealing procedure. In this manner, structural and energetic evolvement with temperature (above T_g) may be observed occurring during passage of time, at much lower temperatures. At these low temperatures, the smearing effects of vibrationally excited modes may be greatly reduced. At the same time, we attempt to clarify why the observed Boson peak (i.e., the excess vibrational density of states over the Debye level at low frequencies) is more enhanced for hyperquenched glasses (HQG) (glasses far from equilibrium) than for the 'standard' glass (glass cooled at 0.167 K·s^{-1}), and how the Boson peak of the HQG decreases with increasing the degree of annealing[9-11]. Recently, we have taken advantage of the HAC approach to investigate the glass transition of water[6-7], and to explore the secondary relaxation process both in the strong glass former GeO_2[12a], and in the methodic glass $La_{35}Al_{25}Ni_2O$[12b]. Besides its scientific importance, relaxation in HQG plays an important role in many practical aspects, e.g., in control of physical properties of different types of glasses, determination of the cooling rate of glass fiber forming, and optimization of the preservation techniques of food and drugs.

In this paper, main results in the field of relaxation in HQGs will be reviewed. Methods for determining T_f will be briefly presented. It will be described how the relaxation features of HQGs are related to the energetic and structural heterogeneity. It will be described how our findings about the relaxation features in hyperquenched silicate glasses, and, in particular the annealing induced pre-endotherm ('shadow' of the glass transition), are used to clarify the glass transition of water. The striking differences in relaxation between strong and fragile HQGs will be shown and the origin of those differences will be discussed. The progress in modeling the enthalpy relaxation of the HQGs subjected to different degrees of annealing will be briefly mentioned. Recently, the HAC approach has been used to study the secondary relaxation in both strong and fragile glass formers, and main conclu-

sions will be given. Finally, some promising observations will be introduced regarding the vibrational properties both in the HQGs subjected to different degrees of annealing and in the nanocrystalline alloys obtained from hyperquenched metallic glasses.

2 Experimental approaches

This paper deals with six different glasses that undergo hyperquenching, annealing and calorimetric scanning. The first glass has the basalt-like composition used for making insulation wool fibers: which is 45.8 SiO_2, 14.9 Al_2O_3, 7.6 FeO, 14.3 CaO, 10.9 MgO, 2.0 Na_2O, 1.0 K_2O, 1.6 TiO_2 and 0.4 P_2O_5 (wt%)[7]. The wool fibers with an average diameter of 4 ~ 15 μm were obtained by spinning the glass melt using the wheel centrifugal process at a rotating speed of about 6 000 $r \cdot min^{-1}$, and hence, got hyperquenched (HQ). This type of glass is here referred to as the basaltic hyperquenched glass (HQG). The second composition has the basaltic composition of the natural glass fibers found in the Kilauea volcano in Hawaii: 49.4 SiO_2, 12.8 Al_2O_3, 2.3 TiO_2, 11.2 FeO, 10.6 CaO, 8.0 MgO, 2.1 Na_2O, and 0.4 K_2O (wt%). The Hawaii fibers were hyperquenched as molten lava is thrown into the air and stretched during explosive eruptions. This type of glass is, in this paper, referred to as the Hawaii HQG. The cooling rates of the basaltic and the Hawaii sample are calculated in the next section. The third glass has a composition of the calcium metaphosphate CaP_2O_6[13]. The HQ glass of this composition was obtained by continuously drawing fibers from the melt through the die (2 mm in diameter) on the bottom of a platinum/rhodium crucible at a cooling rate of about 10^4 $K \cdot s^{-1}$. This type of glass is here referred to as HQCaP_2O_6. The fourth glass is one of the strongest glass system GeO_2[14]. Its hyperquenched state was obtained also by continuously drawing fibers from the melt at a cooling rate of 10^4 $K \cdot s^{-1}$. This type of glass is here referred to as HQGeO_2. The fifth glass has a composition of 74 SiO_2, 16 Na_2O, 4 CaO, and 6 FeO (wt %) with 32% enrichment of iron in the resonant ^{57}Fe isotope[10]. Hyperquenched samples were produced by quenching a thin melt film (approximately 100 to 200 μm in thickness) of melt at 1 500 ℃ into water at an estimated cooling rate of 2×10^4 $K \cdot s^{-1}$. This type of glass is here referred to as HQSilicate. The sixth glass is an alloy system with the composition of $Fe_{90}Zr_7B_3$ with 63% enrichment of iron in the ^{57}Fe isotope[11]. A 20 μm thick ribbon was obtained by the melt-spinning technique. The nanocrystalline material was obtained by heat-treating the HQ glass sample at various temperatures for different durations. This type of the crystalline sample is referred to as NC-FeZrB. The determination of the cooling rate of HQ glasses is described in [15-16] and briefly described in the next section.

Some of the HQ samples were directly measured using the differential scanning calorimeter (DSC) (Netzsch STA 449 C Jupiter). But most of them were annealed before the DSC measurements. The annealing experiments were carried out in an annealing furnace at selected temperatures T_a below T_g for various duration t_a. To determine the cooling rate of the HQGs, the viscosity data should be measured. The high and low temperature viscosity data are measured using a concentric cylinder and a penetration viscometer, respectively[16].

To study the enthalpy relaxation of both annealed and not annealed HQ glasses, the isobaric heat capacities (C_p) of those glasses were measured as a function of temperature by using the DSC. The samples were placed in a platinum crucible situated on a sample holder of the DSC at room temperature. The samples were held for 5 min at an initial temperature of 333 K, and then heated at a standard rate of 0.167 or 0.333 $K \cdot s^{-1}$ to a temperature above the offset temperature of the glass transition, and then cooled back to 573 K at a rate of 0.333 $K \cdot min^{-1}$ to 573 K, thus forming the "standard" glass (SG). After natural cooling to room temperature, the second upscan was performed using the same procedure as for the first. To determine the C_p of the samples, both the baseline (blank) and the reference sample (sapphire) were measured. To confirm reproducibility, the measurements for some samples were repeated to check for drift in the baseline. All the measurements were done in argon to prevent the oxidation of the samples. The details of the measurement conditions are described in the figure captions.

The vibrational density of states (VDOS) both in the HQSilicate sample and in the NC-FeZrB sample was measured using nuclear inelastic scattering[10-11] at the Nuclear Resonance beam line[17] ID18 of the European Synchrotron Radiation Facility (ESRF). The technique provides

partial density of states of the resonant ^{57}Fe atoms with precise calibration of the DOS in absolute meV^{-1} units. The details of the method can be found elsewhere[18]. The measurements on the HQSilicate and the NC-FeZrB samples were performed at room temperature with 0.5 and 1.0 meV energy resolution, respectively. For a comparison between the sample and bulk iron, the DOS of an α-Fe foil was also measured[11].

3 Calorimetric studies of HQGs

3.1 Fictive temperature and cooling rate of HQGs

Mineral basalt is an excellent raw material for making insulation wool fibers with high temperature stability[19]. Due to the fast melt spinning process, the wool fibers are typical hyperquenched glasses, and hence, are suitable objects to study the relaxation phenomena in glasses far from equilibrium and to gain information about the energy landscape of the glasses with high fictive temperatures T_f[9,20]. The typical features of the wool fibers (i.e., the so-called basaltic HQG) during a DSC upscan are displayed in **Figure 1.** The figure shows a broad enthalpy relaxation, the glass transition, two distinct crystallization peaks, and a melting peak. It is clearly seen that the glass has a high tendency to crystallize. This is one of the factors responsible for the high-temperature stability of the basaltic wool fibers[19], which is why such fibers can be used as a good fire barrier. In this paper, the present author will, however, focus on the low temperature exothermic peak indicated by the dashed box (**Figure 1**), which represents the energy release of the HQG during the DSC upscan. The inset of **Figure 1** shows the magnified version of the enthalpy relaxation, which is the basic diagram of the present paper.

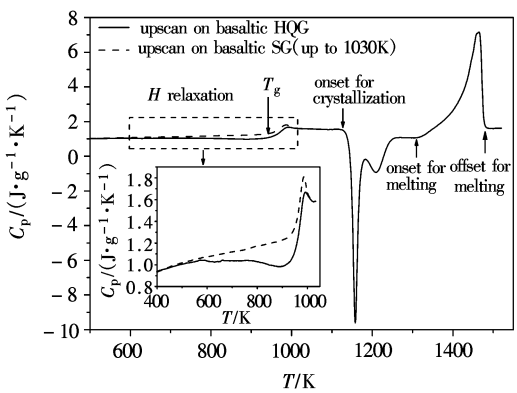

Fig.1 Complete DSC 0.167 K·s^{-1} upscan of the basaltic HQG sample showing broad enthalpy (H) relaxation (weak on this scale) followed by glass transition that ends at 1 030 K, crystallization at 1 156 K, and finally liquidus temperature at 1 484 K. Solid curve: Upscan curve for the basaltic hyperquenched glass (HQG), i.e., the fresh fiber sample. Dashed line: Upscan curve for the basaltic "standard" glass (SG) (see text).
Inset: *H* relaxation diagram magnified from the boxed area of main figure, in which the quenched-in enthalpy is completely released during the first upscan up to 1 030 K. The onset T_g of the upscan curve of the SG sample is 941 K. The area between the dashed and solid curves represents the energy difference between the HQG and the SG sample, and is found to be 64 J·g^{-1}·K^{-1}.

To study the enthalpy relaxation in a HQG, the first thing one needs to do is to determine the fictive temperature and the cooling rate of the glass samples. To do so, we developed a simple and relatively accurate method that is described in [15-16]. Here this paper describes only the main procedures of determination of the cooling rate of HQGs and give two examples of that. The details can be found in [15-16].

Figure 2 shows the enthalpy-matching method, by which the fictive temperature T_f can be obtained. Area A between the C_{pl} curve of the basaltic HQG and the C_{pl} curve of the basaltic "standard" glass (SG) (cooled at 0.33 K·s^{-1}) is the excess enthalpy trapped during hyperquenching process relative to the enthalpy of the SG. If area A is filled in between C_{pl} and C_{pg} curves, area B is obtained, the right borderline of which is actually the T_f of the HQG, i.e., 1 155 K (see **Figure 2**).

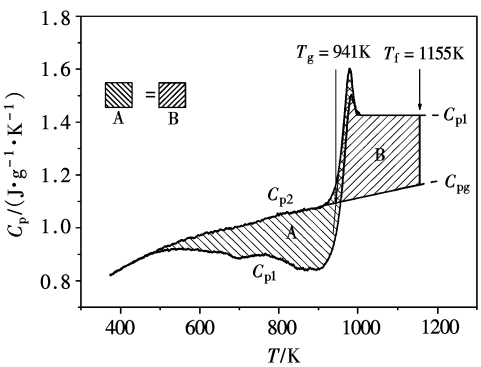

Fig.2 Determination of fictive temperature (T_f) of the basaltic HQG by using the energy-matching method. The figure is re-plotted from [16]. C_{pl} and C_{p2} represent the isobaric heat capacity curves obtained from the basaltic HQG and the basaltic SG sample, respectively, during the DSC upscans at 0.167 K·s^{-1}. The samples are cooled in the first and second DSC down scans at 0.167 K·s^{-1}. C_{pl} and C_{pg} are the liquid and glass heat capacities, respectively. The glass transition temperature T_g and the fictive temperature are found to be 941 and 1 155 K, respectively.

The method for determining T_f is based on the relationship[15]:

$$\int_{T_c}^{T_{eq}} (C_{p2} - C_{p1})\mathrm{d}T = \int_{T_{g,ref}}^{T_f} (C_{p1} - C_{pg})\mathrm{d}T, \quad (1)$$

where T_c is the onset temperature, at which the release of enthalpy starts, C_{p1} and C_{p2} are the heat capacity curves obtained from the first and second DSC upscans using 0.167 K/s, respectively, T_{eq} is the temperature, at which $C_{p2} = C_{p1}$, and C_{p1} and C_{pg} are the liquid and glass heat capacities, respectively. To obtain C_{pg} values above $T_{g,ref}$, the following equation, which describes the temperature dependence of C_{pg}, is used:

$$C_{pg} = a + bT + c/T^2 + d/T^{0.5}, \quad (2)$$

where a, b, c and d are constants.

To determine the cooling rate q_c, at which a glass is hyperquenched, we established a simple relation[16]:

$$\log q_c = 11.35 - \log\eta(T_f), \quad (3)$$

where $\eta(T_f)$ is the viscosity of the glass at the temperature $T = T_f$. When the T_f and the $\log\eta$ vs T relation have been determined, q_c can be calculated from **Equation** (3). In this work, the $\log\eta$ vs T relation is described by the Avramov-Milchev (AM) equation[21-23]:

$$\log\eta = \log\eta_0 + (12 - \log\eta_0)\left(\frac{T_g}{T}\right)^F, \quad (4)$$

where η_0 is a pre-exponential factor, which is the viscosity at infinite high temperature, T_g is the glass transition temperature, and F is the fragility index.

Figure 3 shows viscosity data of the basaltic melt studied in this work and their fit to **Equation** (4). From **Equation** (4), the viscosity at $T = T_f = 1\,155$ K is found to be about 2×10^5 Pa·s^{-1}. By introducing this viscosity value into **Equation** (3), the cooling rate of the basaltic HQG is found to be approximately 10^6 K·s^{-1}. Similarly, the cooling rate of the Hawaii HQG is found to be about 2×10^4 K·s^{-1} as shown in **Figure 4.** The inset of the figure demonstrates how to obtain the T_f value of the Hawaii HQG. In both **Figures 3 and 4**, the viscosity data in the middle range temperature are not available because of the crystallization of the basaltic liquid that hinders the viscosity measurements. On the other hand, reproducible, accurate viscosity data were obtained both on the liquids above their liquidus temperatures (T_{liq}) and on the supercooled liquids above T_g so that reasonable fitting parameters of **Equation** (4) were achieved, and hence, used for determining the cooling rate of the HQGs.

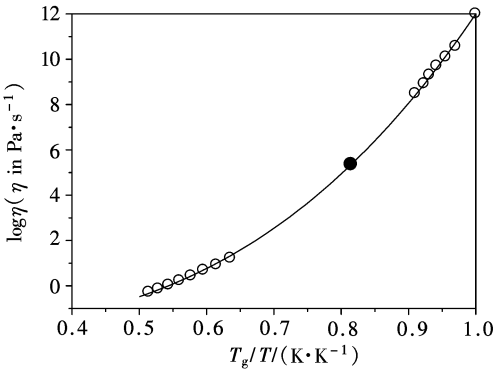

Fig.3　The fragility plot representing the non-Arrhenian degree of the relation between the logarithmic viscosity ($\log\eta$) versus the T_g scaled temperature (T) for the basaltic sample. Open circles: The viscosity data measured in high and low temperature regions using a concentric cylinder viscometer and a penetration viscometer, respectively[17]. Solid line: The fit of the data to the AM equation, i.e., Eq. (4). Solid circle: Viscosity corresponding to the fictive temperature (T_f) of 1 155 K. From this viscosity, the cooling rate (q_c) of the sample is calculated to be ~ 10^6 K·s^{-1} according to Eq. (4).

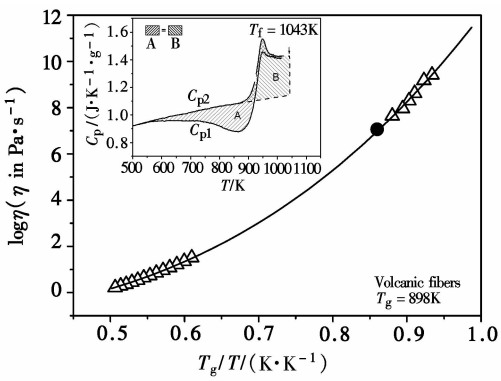

Fig.4　The fragility plot for the Hawaii volcanic glass melt (its composition is given in the experimental part). Inset: The enthalpy relaxation plot, from which the fictive temperature (T_f) is determined to be 1 043 K. Open triangles: The viscosity data measured in high and low temperature regions using a concentric cylinder viscometer and a penetration viscometer, respectively[25]. Solid line: The fit of the data to the AM equation, i.e., Eq. (4). Solid circle: The viscosity corresponding to the T_f of 1 043 K. From this viscosity value, the cooling rate (q_c) of the sample is calculated to be ~ 2×10^4 K·s^{-1} according to Eq. (3).

3.2　Effect of annealing on the enthalpy relaxation of HQGs

Enthalpy relaxation in glass refers to the enthalpy recovery process, i.e., the change of enthalpy from the level of a certain fictive temperature (T_f) to that of an actual temperature, which occurs during both dynamic heating and static annealing. This change is usually detected and recorded by a DSC. T_f refers to the temperature at which the equilibrium state of the original liquid is frozen in dur-

ing the hyperquenching. In most cases, enthalpy relaxation is a non-linear and non-exponential process[4,24-25]. Over the past three decades, enthalpy relaxation has been intensively studied both due to its importance for understanding of the nature of glass and the glass transition and due to its practical importance to optimization of mechanical and optical properties of glass products. Most of these studies have focused on slowly cooled glasses by performing annealing procedures. In the meantime, theoretical approaches to describe the enthalpy relaxation of slowly cooled glasses have been established, by which the calorimetric response to annealing temperature can be well modeled. In contrast, the enthalpy relaxation in hyperquenched glasses (HQGs) such as oxide glass fibers[26], ribbon metallic glasses[27] and organic glass formers[28] have been studied to some extent, and the existing models have failed to describe the enthalpy relaxation of the annealed or partially annealed HQGs[26]. Recently, we have noticed that the enthalpy relaxation in HQGs is attracting attention of both theorists and experimentalists, and promising results have been reported[29-30]. For instance, modeling of the annealing induced pre-endotherm (in some cases, called prepeak or 'shadow' glass transition) in HQGs becomes possible, at least in the case of fragile systems. However, the physical foundation of such modeling still needs to be established. The present paper skips the presentation of the modeling work and, instead, focuses on presentation of our experimental results mainly related to calorimetric studies on both the as-prepared and the annealed HQGs.

To examine how glasses that are trapped in high potential energy states by hyperquenching recover equilibrium states that are lower on the potential energy landscape[9], we first need to measure the C_p upscan curve of the 'standard' glass (SG), i.e., a glass that has been cooled from the liquid to the glass state at a rate of $0.167\ K\cdot s^{-1}$. Both standard glass and HQG are upscanned in a DSC at a rate of $0.167\ K\cdot s^{-1}$. Then we compare both upscans as illustrated in **Figure 5.** The figures shows the difference in C_p between the basaltic SG and the basaltic HQG sample, i.e., $\Delta C_p = C_{p2} - C_{p1}$ as a function of T(see the inset of **Figure 5**). ΔC_p is also referred to as the energy release function, since it represents the rate of the excess energy release from the sample[6]. The total energy stored during hyperquenching is calculated by integrating ΔC_p over the entire temperature range of the measurement, and this gives $64\ J\cdot g^{-1}$. In **Figure 5**, the $\Delta C_p(T)$ function implicitly exhibits a distribution of the excess energy over all configurational coordinates. The existence of the 'shoulder' suggests that two types of structural relaxation below T_g overlap with each other.

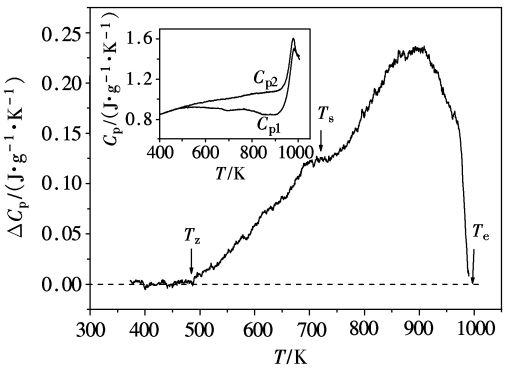

Fig.5 Difference in the isobaric heat capacity between the basaltic SG and the basaltic HQG sample, i.e., $\Delta C_p = C_{p2} - C_{p1}$, obtained from the first DSC upscan (see the inset of the figure) as a function of temperature (T)[6]. Both up-and downscan rates are $0.167\ K\cdot s^{-1}$. T_z is the onset temperature, at which the excess potential energy of the HQG sample relative to the potential energy of the SG sample starts to be released. T_s is the temperature, at which a "shoulder" appears.

Three characteristic temperatures are identified in **Figure 5.** The first one is the onset temperature $T_z(=0.52\ T_g)$, at which the enthalpy starts to release, meaning that the fictive temperature begins to drop. The second one is the "shoulder" temperature $T_s(=0.72\ T_g)$, which implies an overlap of two relaxation processes of the HQG. The third one is the equilibrium temperature $T_e(=1.06T_g)$, at which the quenched-in energy is completely released, i.e. $C_{p1} = C_{p2}$. At T_e, the liquid returns to internal equilibrium. The excess energy of the HQG relative to the SG is a consequence of freezing-in of the configurational states at $T = T_f$, and is approximately proportional to T_f-T_g,. The most excited states are so unstable that the temperature T_z well below T_g, which corresponds to the kinetic energy $1/2k_bT_z$(where k_b is the Boltzmann constant), drives the glass to an energy level corresponding to the real temperature T. T_z decreases with increasing cooling rate, and hence, with increasing T_f. The dependence of T_z on T_f involves three cases. First, when a liquid is cooled at a rate higher than the standard rate $0.167\ K\cdot s^{-1}$, T_f is higher than T_z. Second, when a liquid is cooled at the standard rate, T_f and T_z tends to approach T_g. Third, when a liquid is cooled at a rate below the

standard rate, T_z does not exist, since no energy release takes place. Instead, an enhancement of the T_g peak would occur, and thus T_f should be lower than T_g. According to [22], T_z decreases with increasing cooling rate, and hence, with increasing T_f. However, two important questions need to be answered in the future: a) what is the quantitative relationship between T_z and T_f? b) are there limiting values for both T_z and T_f?

Another important question about the enthalpy relaxation in HQGs is how the annealing process below T_g influences the subsequent calorimetric signals of the annealed HQG during a DSC upscan, i.e., a dynamic heating. **Figure 6** illustrates the upscan C_p curves of the basaltic HQG annealed at various temperatures T_a for an annealing time of $t_a = 8$ days. The thick curve is the C_p curve of the basaltic SG sample. When increasing T_a, the energy release peak (or so-called exotherm before T_g) is gradually decreased from the left side to the right, i.e., the left cutoff of the exotherm shifts to higher temperatures, until the peak completely disappears. During the annealing process, the structural configuration with a higher energy is transformed into that with a lower energy. T_a determines the extent of changes in the structural configuration during annealing. The vibrational excitation energy required for the change in the structural configuration depends on its energy level. All configurational states approach the energy level corresponding to the annealing temperature, and this takes long time. The shift of the left foot of the exotherm to higher temperatures is due to the fact that more and more low energy basins of the energy landscape are sampled by the system when increasing T_a.

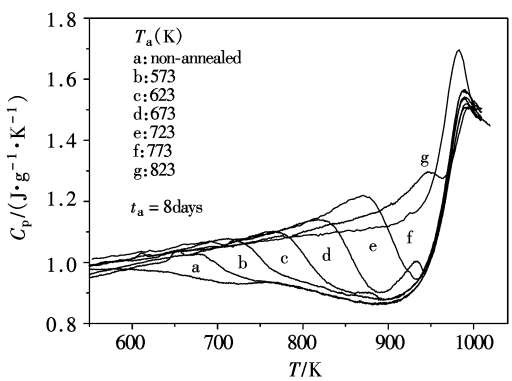

Fig. 6　The C_p curves obtained from the DSC upscans of the basaltic HQG sample, after an annealing treatment of $t_a = 8$ days at the temperatures (T_a) shown in the legend. The thick curve is the C_p curve of the basaltic SG sample. Both up- and downscan rates are 0.33 K·s^{-1}

In **Figure 6**, it is furthermore seen that, when T_a is sufficiently high (but below T_g), a pre-endotherm occurs below the onset temperature of the exotherm. The higher T_a is, the higher and the broader the endotherm becomes. At the same time, the endotherm gradually shifts to higher temperatures, but at the expense of successive loss of the left part of the exotherm. In a certain range of T_a, the exotherm and endotherm co-exist on the C_p curve, that leads to the occurrence of the crossover point between the C_p curve of the annealed HQG and that of the SG.

Figure 7 shows the effect of t_a on the calorimetric response of the basaltic HQG at $T_a = 723$ K. When the annealed sample is heated from room temperature to T_e, a pre-endotherm appears followed by an exotherm. The pre-endotherm becomes more and more pronounced with t_a, and it shifts to higher temperatures until the exotherm disappears. This implies that, after sufficient annealing, the potential energy of some weak structural domains in the HQG falls down to a level below that of the SG, and tends to the final level corresponding to the given T_a, while the potential energy of some strong structural domain remains higher than that of the SG.

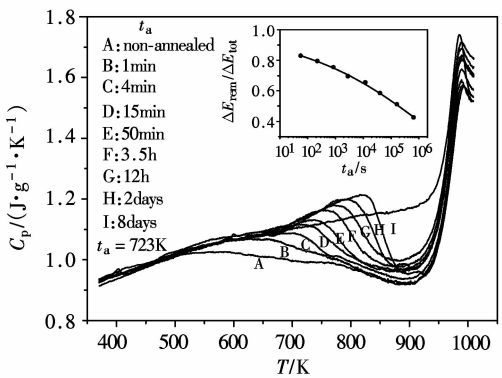

Fig. 7　The C_p curves obtained from the DSC upscans of the basaltic HQG sample, after an annealing treatment at the temperature $T_a = 723$ K for the durations designated in the legend. The thick curve is the C_p curve of the basaltic SG sample. Both up-and downscan rates are 0.33 K·s^{-1}. Inset: $\Delta E_{rem}/\Delta E_{tot}$ as a function of t_a, where ΔE_{rem} is the energy remaining in the fibers after annealing, and ΔE_{tot} is the total energy stored during the HQ process. Solid line in the inset is obtained by fitting the experimental data to the Kohlrausch equation[6]

The t_a dependence of the energy release rate at a constant T_a reveals that it takes a long time for all configurations to find the lowest minima, although they are subjected to the same excitation energy. This also means that there is a broad distribution of relaxation times, the width

of which is determined by the diversity of configurational states. The pre-endotherm becomes deeper as t_a extends. At a given T_a, the vibrational density of states in HQGs decreases with t_a[9,20].

The inset of **Figure 7** shows the effect of t_a on the remaining energy, ΔE_{rem}, normalized by the total energy stored during hyperquenching, ΔE_{tot}. The solid line is the fit of the experimental data to the Kohlrausch function $\Delta E_{rem}/\Delta E_{tot} = \exp[-(t/\tau)^{\beta}]$, where τ is the characteristic, temperature-dependent relaxation time, and $\beta \in (0,1)$ is the stretching exponent describing the broadness of the relaxation time distribution. In **Figure 7**, a value of $\beta = 0.16$ is obtained for $T_a/T_g = 0.66$[6], which is much lower than those reported by other authors for the energy landscape-influenced regime ($0.45 < T/T_g < 1$)[31]. This small β value of the HQG is attributed to its larger configurational entropy in comparison to the SG. The small β value also indicates that the distribution of relaxation times of the HQG during annealing at 723 K becomes more stretched in comparison with that of the SG.

From the HAC studies, we can obtain abundant information on the energy that can be trapped into glasses by hyperquenching, relative to the SG, and on the magnitude of barriers separating basins of attraction on the landscape. Stepwise annealing studies give information on the matter of energy heterogeneity and the question of "nanogranularity" in liquids near T_g.

During annealing, the relaxing part of microstructures becomes less disordered and more stable in comparison to those of the 'standard' glass. When the hyperquenched, annealed glass is upscanned in the DSC, the degree of disorder in the relaxing part of the structure increases and gradually approach that of the standard glass. This process leads to an endothermic event, i.e., to the pre-endotherm. The extent of the pre-endotherm increases with increasing T_a and t_a. The pre-endotherm only occurs when the glass is hyperquenched and then annealed. The pre-endotherm is more pronounced for glasses with a higher fictive temperature (T_f) than those with lower T_f, when the annealing conditions are the same. Recently, the annealing-induced pre-endotherm has also been studied by means of the molecular dynamic simulation on the hyperquenched glassy water[29].

Figures 8 to 10 demonstrate some features of the pre-endotherm of the annealed basaltic HQG[32-35]. Curve 1 of **Figure 8(a)** represents the C_p curve of the HQG annealed for 8 days at 773 K, which exhibits a pronounced pre-endotherm. As shown by curve 2 of **Figure 8(a)**, this pre-endotherm can be completely removed when the annealed HQG is reheated to the crossover temperature ($T_{cross} = 897$ K), then cooled back to room temperature, and finally re-upscanned to the maximum temperature. At the same time, the exotherm remains unaffected. Curve 3 of **Figure 8(a)** is the C_p curve of the standard glass. The removal of the pre-endotherm by the partial annealing is also seen in **Figure 8(b)**. The figure shows a clear disappearance of the pre-endotherm and the remaining exotherm. In addition, the pre-endotherm can also be partly eliminated by heating the glass to a temperature below T_{cross}, e.g., to 857 K and cooling it back to RT, and reupscan it to the maximum scanning temperature. The partial removal of the pre-endotherm is manifested in **Figure 9**, where a comparison between curves 1 and 2 is made. The exotherm remains completely unaffected, since curves 1 and 2 overlap in the exothermic part.

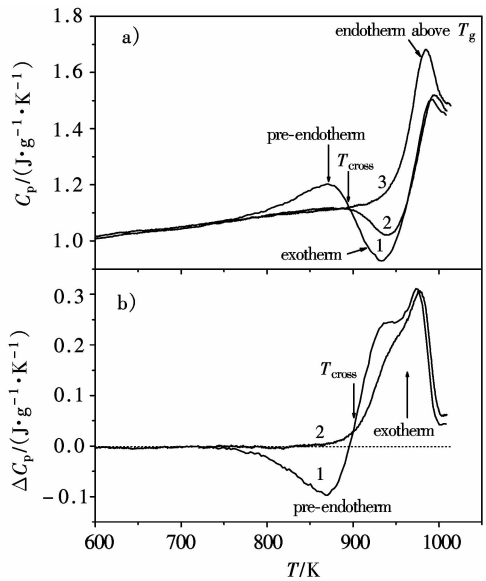

Fig.8 Influence of heating conditions on the DSC pre-endotherm (or the pre-peak) that is caused by a sufficient degree of the annealing process for the basaltic HQG sample [37]. a) C_p as a function of T. Curve 1: C_p of the HQG sample annealed at 773 K for 8 days; Curve 2: C_p of the HQG sample annealed at 773 K for 8 days, and then heated from 298 K to the crossover temperature (T_{cross}) of 897 K; Curve 3: C_p of the basaltic SG sample. b) Difference in C_p between the basaltic SG and the basaltic HQG sample, ΔC_p, as a function of T. Curve 1: ΔC_p of the HQG sample annealed at 773 K for 8 days; Curve 2: ΔC_p of the HQG annealed at 773 K for 8 days and then heated from 298 K to the T_{cross}. The DSC up-and downscan rates are 0.33 K·s^{-1}. Dotted line: $\Delta C_p = 0$ for the SG sample.

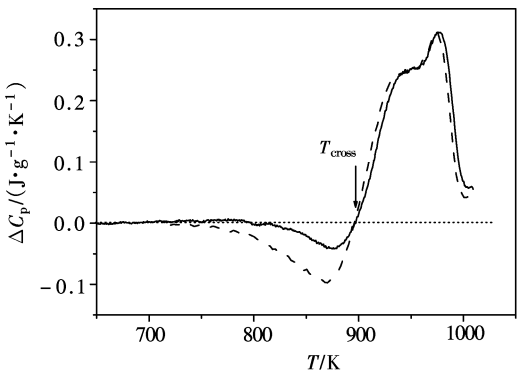

Fig. 9　ΔC_p as a function of T, showing the influence of heating conditions on the DSC pre-endotherm of the annealed HQG sample [37]. Dashed line: ΔC_p of the HQG sample annealed at 773 K for 8 days; Solid line: ΔC_p of the HQG sample annealed at 773 K for 8 days and then heated from 298 to 857 K (a temperature below T_{cross}). The DSC up- and downscan rates are 0.33 $K\cdot s^{-1}$. Dotted line: $\Delta C_p = 0$ for the SG sample

Another interesting feature of the pre-endotherm is its recovery behaviour as shown in **Figure 10.** The pre-endotherm can be recovered (solid curve), when the annealed HQG, the pre-endotherm of which has been lost (dashed curve) during upscanning to T_{cross}, is re-annealed for a given t_a at the same temperature as the previous T_a. Specifically, the HQG was re-annealed for 1 day at 773 K. The recovery of the pre-endotherm would be more pronounced, if t_a were longer. This indicates that during re-annealing some sub-regions in the glass structure relax down to the energy level below that of the standard glass, while some sub-regions keep the energy level above that of the standard glass. This could be attributed to the energetic heterogeneity, non-linearity, and non-exponentiality, of the relaxation process[9,25]. It should be noted that the recovery behaviour of the pre-endotherm occurs only when the excess enthalpy remains in glass.

However, the physical origin of the C_p pre-endotherm of the annealed HQG is different from that of the T_g endotherm of the SG. The pre-endotherm can be eliminated and then recovered by properly choosing heating and re-annealing procedures. In contrast, the T_g endotherm is not removable by heating and annealing processes, instead, it always occurs during up-and downscan as long as crystallisation is avoided. The T_g endotherm is caused by a transition between glass and liquid, which is accompanied by an abrupt increase in configurational entropy. In contrast, the occurrence of the pre-endotherm is a signature of the strong non-exponential relaxation of the HQGs during annealing. It reflects the higher configurational entropy, and larger energetic and structural heterogeneity of the glass at $T = T_f$ compared with a glass at $T = T_g$. As described in [7], all glasses have a spectrum of relaxation times, as if composed of many microglasses of different T_g values. The onset temperature of the pre-endotherm (also called 'shadow' T_g) is simply the collective T_g of that component of the HQG that has sufficiently low micro-T_g values to be relaxed by annealing[7].

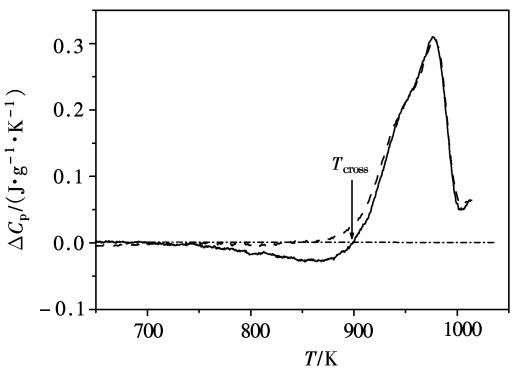

Fig. 10　ΔC_p as a function of T, demonstrating the removal and recovery behaviour of the pre-endotherm[37]. Dashed line: ΔC_p of the HQG sample annealed at 773 K for 8 days, then heated from the rool temperature T_{room} (298 K) to T_{cross} (897 K) and then cooled back to T_{room}; Solid line: ΔC_p of the HQG annealed at 773 K for 8 days, then heated from T_{room} to T_{cross}, then cooled to T_{room}, and finally re-annealed at 773 K for 1 day. The DSC up-and downscan rates are 0.33 $K\cdot s^{-1}$. Dotted line: $\Delta C_p = 0$ for the SG sample.

4　Anomalies of relaxation in hyperquenched strong glasses

In **Figures 11(a) and (b)**, ΔC_p is plotted against the DSC upscanning temperature T normalized by T_g, i.e., T/T_g, for both the fragile $HQCaP_2O_6$ and the strong $HQGeO_2$, respectively. The figures show the effect of the annealing temperature T_a on the enthalpy relaxation in both glasses. For the fragile $HQCaP_2O_6$ (**Figure 11(a)**), the ΔC_p peak gradually disappears from low to high temperature until the entire ΔC_p peak disappears with increasing T_a ($< T_g$) for $t_a = 12$ h. Consequently, the left cutoff of the peak shifts to higher temperature, whereas the right cutoff remains unchanged. In contrast, for the strong system $HQGeO_2$ (**Figure 11(b)**), the ΔC_p peak becomes smaller and the left and right cutoffs are getting closer to each other with increasing T_a ($< T_g$) for $t_a = 24$ h.

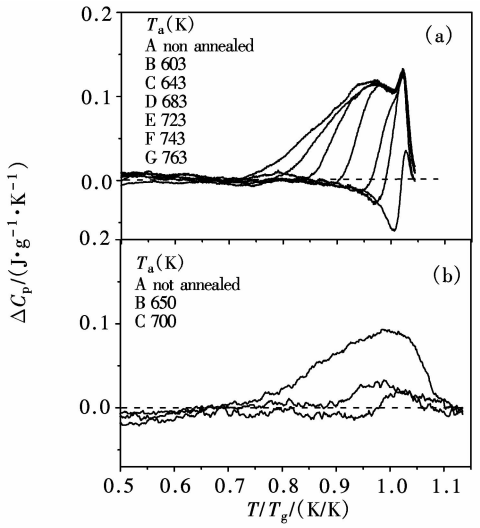

Fig. 11 Comparison in enthalpy relaxation between a HQ fragile system (CaP_2O_6 glass)[14], and a HQ strong system (GeO_2 glass)[15] by performing annealing and subsequently DSC upscanning. (a) Effect of the annealing temperature T_a on the ΔC_p curve of the HQ CaP_2O_6 glass for an annealing time of $t_a = 3$ h. (b) Effect of T_a on the ΔC_p curve of the HQ GeO_2 glass for an annealing time of $t_a = 3$ h. The T_g values of the CaP_2O_6 and the GeO_2 glasses are 797 and 830 K, respectively. The DSC up-and downscan rates are 0.33 $K\cdot s^{-1}$. Dashed line: $\Delta C_p = 0$ for the SG sample

In other words, while a "horizontal" energy release occurs in the fragile glass, a "vertical" energy release occurs in the strong glass. This means that, for $HQGeO_2$, a single annealing temperature (representing the kinetic energy) can induce the release of the potential energy that has a distribution over all microstructural domains (e.g., different bonding types), and hence, over all the sub-fictive temperatures (sub-T_f) since each sub-T_f describes a single microstructural domain. Note that the T_f of a glass is actually the average of all the sub-T_f values. Such relaxation feature confirms that there exists only a single megabasin in a strong system[31], which consists of basins with different depths (bond energy). The depths of the basins are distributed over the collective configurational coordinates, which is indirectly reflected by the distribution of the ΔC_p over T. A single temperature, i.e., a given single excitation energy 0.5 kT_a for a certain t_a is able to cause each microstructural domain (i.e., each bond type) to relax to a certain degree by sampling basins from shallow to deep basins successively. Increasing T_a for a constant t_a leads to an increase in the degree of relaxation by sampling deeper basins. The energy release of $HQGeO_2$ at any T_a below T_g is accompanied by the relaxation of all the structural domains during the annealing process. The degree of the relaxation of these domains (e.g., the two adjacent GeO_4 tetrahedra with different Ge-O-Ge angles) towards a total relaxation is determined by both T_a and t_a. The similar relaxation phenomena are also observed for the $HQSiO_2$ glass ($HQSiO_2$), which indicates that the 'vertical' relaxation is a universal feature of strong glasses [14].

However, as shown in **Figure 11(a)**, the relaxation of the fragile systems proceeds in the manner that some microstructural domains relax, whereas some remain unaffected. This feature of relaxation agrees with the illustration given in [31] about the energy landscape of the fragile systems, which displays a proliferation of well-separated megabasins. It also implies that the energetic and structural heterogeneity of the fragile $HQCaP_2O_6$ at $T = T_f$ is higher than that of the strong $HQGeO_2$. Potential energy, relaxation and vibrational dynamics of the fragile systems are discussed in detail in [9,20]. In addition, **Figures 11(a) and (b)** exhibit another pronounced difference in the enthalpy relaxation between the fragile and strong systems. In the annealed $HQCaP_2O_6$, an pre-endotherm (sometimes referred to as pre-peak) is observed (see the peaks underneath the ΔC_p zero line) before the exothermic energy release peak occurs, when T_a is sufficiently high but below T_g. The extent of the pre-endotherm can be enhanced by raising T_a. The origin of such pre-endotherm has been discussed in [7]. However, the pre-endotherm is not observed on the $HQGeO_2$ (see **Figure 11(b)**). The lack of the pre-endotherm in the ΔC_p curves is another evidence for less energetic and structural heterogeneities in strong glasses than in the fragile glasses.

In **Figures 12(a) and (b)**, ΔC_p is plotted against the DSC upscanning temperature T normalized by T_g, i.e., T/T_g, for both the fragile $HQCaP_2O_6$ and the strong $HQGeO_2$, respectively. The figures show the effect of the annealing time t_a on the enthalpy relaxation. Similar to the consequence of an increase of T_a, an increase of t_a results in "horizontal" relaxation patterns for $HQCaP_2O_6$ (**Figure 12(a)**), and in "vertical" relaxation patterns for $HQGeO_2$ (**Figure 12(b)**). This indicates that the influence of t_a on the potential energy landscape of the strong systems differs from that of fragile ones. For the fragile

$HQCaP_2O_6$, at a fixed T_a, i.e., a fixed kinetic energy, prolonging t_a causes an increase in the probability for a microstructural domain of the glass to escape from a basin located at higher levels of megabasin towards another basin located at lower levels of megabasins, until all domains fall down to the energy level that the T_a determines (i.e., the rate of the escape depends on T_a). When a basin is sampled, its neighbored basin is influenced and sampled. In other words, neighbored basins are sampled after one another. Such influence could be the origin of the "horizontal" decrease in the excess energy (i.e., the area under the ΔC_p curves). In contrast, for strong systems, the basins with a certain range of depths are independently sampled by different types of microstructural domains (GeO_4 tetrahedra with different Ge-O-Ge angles, and different bonding energies) during a given t_a. By extending t_a, the deeper basins get a chance to be sampled. From the microstructural pint of view, during annealing of the fragile HQG, the severely broken or distorted bonds are restored, whereas the slightly broken bonds remain unaffected. This means that the structural relaxation is of more heterogeneous nature. By contrast, during annealing of the $HQGeO_2$, it is of more cooperative feature with respect to the relative uniform microstructural domains (i.e., less bond types). The cooperative relaxation is associated with the coupled rotations of GeO_4 tetrahedra and interaction between different bonds (i.e., bonds with different potentials). At a single T_a, the coupled motion of bonds from non-equilibrated (or heavily distorted arrangements) to relatively equilibrated states (or distorted arrangement) causes a certain extent of relaxation of the entire structure. That is why relaxation in $HQGeO_2$ takes place during the entire T range, in which the ΔC_p peak is situated.

During relaxation, the energy transition of the local structural units takes place between different basins via breaking and reforming of bonds. Different local minima can be identified as different bonding forms, and then the energy of minima coincides with the potential energy of the configurations, i.e., with the number of bonds[36]. The structural change over t_a is a kinetic process, during which a gradual increase occurs in population of microstructural domains that participate in jumping from higher to lower minima. This causes a 'vertical relaxation'. Such jumps affect each other. In other words, cooperative relaxation processes take place in strong HQGs.

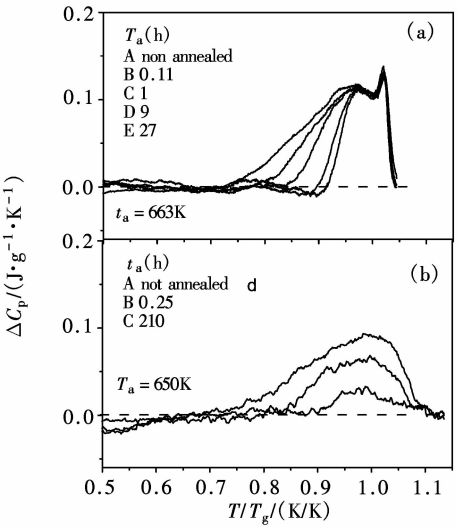

Fig. 12　Comparison in enthalpy relaxation between a HQ fragile system (CaP_2O_6 glass), and a HQ strong system (GeO_2) by performing annealing and subsequently DSC upscanning. (a) Effect of the annealing time t_a on the ΔC_p curve of the $HQCaP_2O_6$ glass for an annealing temperature of T_a = 663 K. (b) Effect of t_a on the ΔC_p curve of the $HQGeO_2$ glass for an annealing temperature of T_a = 650 K. The DSC up-and downscan rates are 0.33 $K\cdot s^{-1}$. Dashed line: $\Delta C_p = 0$ for the SG sample

Furthermore, for a comparable degree of annealing (i.e., same T_a/T_g), the pre-endotherms appear for the fragile $HQCaP_2O_6$, whereas they do not appear for the strong $HQGeO_2$(**Figures 12(a) and (b)**). This confirms again that, during annealing, the structural relaxation is of more cooperative or connective nature in the strong system than in the fragile systems. The finding of such features is not only of scientific importance, but also of potential technological importance. The optical and mechanical properties of glass fibers are strongly influenced by their thermal history (e.g., cooling rate and the annealing degree) and mechanical history (e.g., drawing stress). The knowledge about relaxation of the $HQGeO_2$ and $HQSiO_2$ fibers may contribute to optimization of the forming and annealing processes of the GeO_2/SiO_2 fibers with respect to their optical and mechanical performances.

In summary, hyperquenched strong systems exhibit three anomalies of the enthalpy relaxation during the annealing process in comparison to relative fragile glasses. The first anomaly is that the ΔC_p curve of hyperquenched fragile systems can be deconvoluted into a low and a high T Gaussian distributions, whereas that of strong systems can be described by only one Gaussian distribution. The

second anomaly is that, with increasing T_a and t_a, the excess energy is released 'horizontally', i.e., from lower to higher T in the hyperquenched fragile glasses, whereas it is released 'vertically', i.e., from higher to lower ΔC_p in the hyperquenched strong glasses. The third anomaly is that a pre-endotherm appears on the C_p curve of a fragile system, whereas it does not appear on that of a strong system. The qualitative clarification of those anomalies may be achieved in terms of the potential energy landscape. All those anomalies reflect the difference in the mechanism of structural rearrangements during dynamic heating or annealing between the two systems. The anomalies imply that the relaxations of different bonding situations in hyperquenched fragile systems are of independent nature, while those in hyperquenched strong systems are of cooperative nature. It also indicates that fragile systems possess a higher degree of the structural heterogeneity than strong ones.

To further explore the correlations between the liquid fragility on the enthalpy relaxation in HQ glasses, we have studied a large number of glass systems with different fragilities by means of the HAC approach[12-14,30,35]. It is found that two main distributions of relaxation times determine the shape of the excess ΔC_p curves of the annealed HQGs. One distribution is associated with the β relaxation (of the network modifiers and non-bridging oxygen ions in silicate glasses) that causes the low T relaxation well below T_g. The other is associated with the α relaxation (of the structural network in silicate glasses) that causes the high T relaxation around T_g. The ratio between the contribution of the β relaxation and that of the α relaxation increases with an increase of the liquid fragility. Based on these results, we have established a relaxation time function and combine it with the existing TNM model[24-25] to model the complex the C_p curve of the HQGs with different degrees of annealing. Recently, we have succeeded in accurately modeling the enthalpy relaxation response to both dynamic heating and static annealing for several fragile HQ systems. This is mainly attributed to two major modifications to the existing approaches. The major modification is to introduce the non-Kohrausch composite relaxation function (CRF) that describes two well-separated distributions of relaxation time. Another modification is to take into account the substantial broadening of the glass transition region during the HQ process. Consequently, the predicted C_p curve of the HQGs with different annealing degree is in excellent agreement with that measured using DSC. More importantly, this prediction is made only by changing the cooling rate parameter in the model, keeping all other parameters at the values obtained from the data of the slowly cooled glass. Despite the considerable improvement in modeling relaxation of glasses, it is, in our opinion, crucial to continue the modeling work in three important directions. The CRF should be tested on the mono-component strong glass systems like SiO_2 and GeO_2, since it is not yet possible to model relaxation in these systems. Second, relaxation of other types of glass formers like metallic and molecular systems should be modeled using the improved model in order to judge if the model is universal or not. Third, the physical foundation of the CRF should be explored. Fourth, it should be established whether there are still possibilities to further improve the CRF and to make additional modification to other steps of the modeling.

By applying the HAC approach, we have found that unlike fragile glasses the strong $HQGeO_2$ glass relaxes in a manner that all the secondary relaxation units contribute to the primary relaxation[12]. By analyzing the dynamic properties of the secondary (β) relaxation, we have identified two typical features of the Johari-Goldstein (JG) relaxation in the $HQGeO_2$ glass. First, the quantitative relationship observed here between E_β (activation energy for the β relaxation) and T_g agrees well with the empirical relation of the JG relaxation. Second, the characteristic β relaxation time of the GeO_2 glass at T_g is found to be about 10 s, larger than that of relatively fragile glasses. These results verify that the JG peak in strong glasses is hidden by the α peak in the dielectric loss curves. A detailed discussion about the JG relaxation in the GeO_2 glass was given in[12].

Very recently, the dynamics of the secondary (β) relaxation in HQ metallic glasses like $La_{55}Al_{25}Ni_{20}$ ribbons has been investigated[12b]. The results show that the observed β relaxation exhibits a typical feature of the genuine JG relaxation, i.e., the variation of its activation energy (E_β) with the glass transition temperature (T_g) obeys the relation $E_\beta = 26.8RT_g$. The correlative degree between the β and the primary α relaxations is closely associated with the liquid fragility index. The correlation

$E_\beta = 26.1RT_g$ also applies to the metallic glass in question, indicating that JG relaxations are intrinsic in metallic glass formers.

As mentioned in the experimental part of the paper, the HQ processes of glasses were realized either by centrifugal fiber spinning or by melt film dip into water or by continuous fiber drawing. For the latter process, glasses are thermally hyperquenched and mechanically stretched. Hyperquenching leads to the trap-in of higher enthalpy state in glasses and, thereby, to a higher fictive temperature than the standard quenching ($0.167\ K \cdot s^{-1}$), whereas stretching results in quench-in of structural anisotropy of glasses, i.e., a certain degree of preferred structural orientation (stretched network) along the axial direction of the fibers, which can be quantified by the optical birefringence. Therefore, when the enthalpy relaxation in continuous fiber samples is studied, it is important to take the relaxation of the anisotropic structure into account[37-38]. The results show that, upon static annealing and dynamic heating, both anisotropic structure and enthalpy occur, but the former relaxes considerably faster than the latter. These observations imply that the anisotropic structural relaxation results from fast relaxation of the local structure, while the enthalpy relaxation results from slow relaxation of larger domains of the network. It should be noted that the slow relaxation includes the low T relaxation of network modifiers and non-bridging oxygen ions or the clusters of them, and the high T (near T_g) relaxation of the network skeleton as discussed above.

5 Glass transition of water

Glassy water is the most abundant form of water in the Universe[39], and it is easily formed by molecular deposition on interstellar dust particles that constitute the major component of comets. Beside the molecular deposition, glassy water can also be obtained by hyperquenching liquid water. As is well known, most of glass formers exhibit an endothermic calorimetric glass transition before crystallization. However, it has been debated for more than five decades whether this is also the case for glassy water[7-8,40-49]. For the last 20 years, it has been widely accepted that the glass transition temperature of water is 136 K[42-43]. Recently, this T_g assignment seems rather problematic, when one carefully examines the procedure of the earlier measurements of the water T_g. By comparing enthalpy relaxation data of glassy water with those of some other HQ glasses, it is found that the 136 K assignment could be wrong[45]. The new analysis[45] has led to re-assignment of the water T_g to a higher temperature(165 K).

To further clarify the glass transition of water and verify the new T_g assignment, we have made further efforts[7-8] as described below. First, we looked into the protocols of preparation and characterization of the hyperquenched glassy water (HQGW) samples reported in[42-43]. The HQGW samples were obtained by hyperquenching the liquid water at $10^6\ K \cdot s$, a rate comparable to that estimated for the basaltic HQG studied in this work. Then, the HQGW sample was annealed at 130 K for 90 minutes in order to release the energy stored in the samples during hyperquenching. Otherwise, the endothermic signal would be obscured by the exothermic peak due to the energy release from the HQ state. The annealed samples were upscanned by a DSC at $0.167\ K \cdot s^{-1}$ as shown in the inset of **Figure 13.** From the DSC curves, a rather weak endothermic peak with an onset temperature of 136 K was detected for both the HQGW and the vapour-deposited amorphous solid water (ASW). This peak was considered to be the consequence of the glass transition[43], and hence, the onset temperature 136 K of the peak was assigned to be the T_g of the water. To find whether such an assignment is justified or not, we mimic the experimental protocol of the HQGW on the basaltic HQG samples. The basaltic HQG samples were subjected to a quenching rate of about $10^6\ K \cdot s^{-1}$ comparable to that for HQGW. The basaltic HQG sample was annealed at 823 K for 90 minutes. These annealing conditions are similar to those used for both HQGW and ASW samples. Then, the basaltic HQG sample was upscanned by a DSC at $0.167\ K \cdot s^{-1}$, so that the calorimetric responses, i.e., the C_p curves of the sample were obtained as shown in **Figure 13**. From the C_p curve, a weak endothermic peak, i.e., the above-denominated pre-endotherm, was detected before a strong exothermic peak appears, and it has the same shape as the weak peak of both HQGW and ASW samples shown in the inset of **Figure 13**. The onset temperature of the endothermic pre-peak is identified to be 753 K, which is 20% lower than that of the T_g, i.e., 941 K. For this reason, we also call the pre-endotherm a 'shadow' of the

real glass transition[7]. These findings strongly suggest that the observed endotherm of the glassy water above 136 K also be a 'shadow' of the real glass transition. This substantiates earlier conclusions[7,45] that the real T_g of water cannot be directly probed except by some scaling procedure.

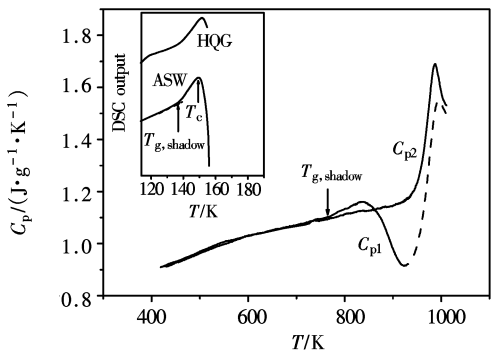

Fig.13 Comparison of DSC upscans of the annealed basaltic HQG with the equivalent DSC upscans of hyperquenched glassy water (HQGW) and the amorphous solid water (ASW)[7]. The basaltic HQG was annealed at 823 K for 90 min before upscanning. C_{p1} and C_{p2} represent the C_p curves obtained on the basaltic HQG and the basaltic SG sample, respectively, at a upscan rate of 0.33 K·s^{-1}. The dashed line is the part that has been cut from the water sample scan by crystallization, commencing at the temperature marked T_c. Inset: The C_p upscan curve of HQGW and ASW samples[46], annealed for 90 min at 130 K before upscanning

In **Figure 13**, it is also seen that the 'real' glass transition in the case of water has been eliminated from observation by crystallization. The ratio of $T_{g,shadow}$ to T_g of the basaltic HQG is 0.80. Applying the same ratio to $T_{g,shadow}$ of water, we obtain a 'real but hidden' T_g of 169 K. However, this ratio will depend on system fragility, so the estimate of the hidden T_g for water is uncertain, and is better estimated by other means[7,45]. The existence of the "shadow" glass transition is also verified by the HAC experiments on other types of samples like the hyperquenched SiO_2-Al_2O_3 binary glass[7] and metallic glasses[27]. Very recently, the shadow glass transition has also been observed in studies on electrospray-quenched molecular glasses of dibutylphthalate and propylene glycol[28]. Therefore, the "shadow" glass transition is probably a universal feature of all the annealed HQGs.

In 1995, Kohl et al observed the enhancement of the endothermic peak in HQGW upon slow cooling from 140 K after a deposition time of 16 min[49]. Based on this observation, they believe that the peak is attributed to the primary relaxation, i.e., the real glass transition. However, the enhancement of the peak that they observed is also the behaviour expected for an annealing pre-endotherm of the basaltic HQG[8]. After all, the simplest way of understanding the existence of the pre-endotherm (or "shadow" glass transition) is to regard them as the annealing-enhanced glass transitions of the short relaxation time components ("microglasses"[9]) of the non-exponentially relaxing macroglass. In **Figure 14**, it can be seen how sensitive the pre-endotherm is to the annealing time for the basaltic HQG sample. The peak can be induced even by a short annealing time, e.g., 8 min. On the other hand, it is also seen how weak the pre-peak is in comparison to the real glass transition peak. These two features are also exhibited by the endothermic peak observed in the DSC curves of the HQGW[49]. Thus, it is further confirmed that the peak that Kohl et al observed is indeed a 'shadow' of the real glass transition. Despite the advances reported above, the debate about the glass transition and the T_g assignment of water will continue, as long as the glass transition cannot be probed directly. Very recently, Angell gave a comprehensive review about several aspects of controversies about the unusual glass forming properties of water[48]. This review is useful for getting a big picture about the glass transition of glassy water and for enhancing the future studies of glassy water.

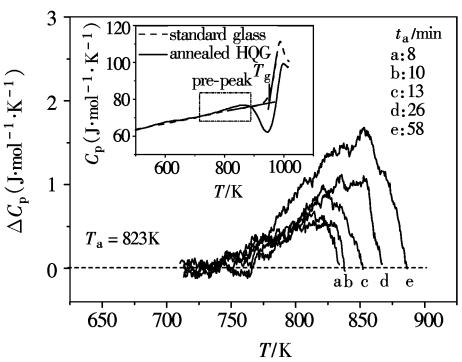

Fig.14 The annealing time (t_a) dependence of the difference in C_p between the basaltic HQG and the basaltic SG sample, ΔC_p, at T_a = 823 K[8]. Inset: The C_p curves for the annealed HQG (solid line) and the SG (dashed line) sample, which were obtained at a upscan rate of 0.5 K·s^{-1}. Boxed area refers to the region, where the pre-endotherm occurs.

6 Vibrational dynamics in HQGs

6.1 Vibrational density of states (DOS) in HQGs

Over the past three decades, vibrational dynamics of glass has been an intensively explored subject due to its

importance for revealing the nature of glass. One of the focuses of this subject is on the origin of the boson peak (BP). BP is a broad peak in the quantity $g(E)/E^2$, where $g(E)$ is the vibrational density of states (VDOS) as a function of the vibrational energy E. Therefore, it represents an excess of states relative to the $g(E)/E^2$ value (= *const*) predicted by the Debye theory. It has been proved that BP is a fundamental feature of all glasses found in the incoherent inelastic neutron scattering and Raman spectra in low frequencies, i.e., at energies in the 2 ~ 10 meV region[50-53]. In contrast, BP is rarely seen in crystals. According to numerous studies[54-59], the BP may have different sources such as large clusters[54], nanoparticles[55], floppy modes[56], mismatched rings[57], the rocking of small tetrahedral groups[58], and connected rings in zeolite[59]. This Boson peak is identified with the existence of intermediate-range order in the glass[60-62]. Furthermore, the intensity of the Boson peak depends on temperature, pressure and the types of glasses.

Until now, most of VDOS studies have been done on the SG sample, i.e., the glasses cooled at the standard rate 0.167 K·s^{-1}. Information obtained from these studies is valuable for understanding the vibrational dynamics of glasses[50]. However, to clarify the origin of the Boson peak and to derive the correlation between the dynamics and thermodynamics of the glass-forming liquids, one should study not only the SG sample, but also the HQG sample. First interesting results have been achieved regarding the T_f dependence of the VDOS in HQGs[9,20], which enhances the understanding of the origin of the Boson peak.

Figure 15 shows the influence of hyperquenching and annealing on the low frequency vibrational mode of glasses, which is detected by means of the cold neutron inelastic scattering time-of-flight measurements. The $Z(\omega)$ function[9,63-65] in the figure may be regarded as an approximate representation of an effective VDOS, $G(\omega)$, ignoring corrections for effects such as multiphonon and multiple scattering. It is noticed that the sharp maximum is developed at a frequency of ~ 40 cm^{-1} in the case of the HQGs. Division of $Z(\omega)$ in Figure 15 by ω^2 would certainly emphasize the excess of the $Z(\omega)$ of the HQG over that of the SG, and therefore it can be stated that the BP has been greatly enhanced in the HQG. In liquids, the BP is obscured by increased quasielastic scattering. Thus, HQGs, in which the high temperature structure is retained but the quasielastic scattering is suppressed, should be optimal objects for studying the Boson peak. In **Figure 15**, it is clearly seen that the BP is reduced with increasing an annealing degree of the HQG, and it disappears when the glass is crystallized to a large extent.

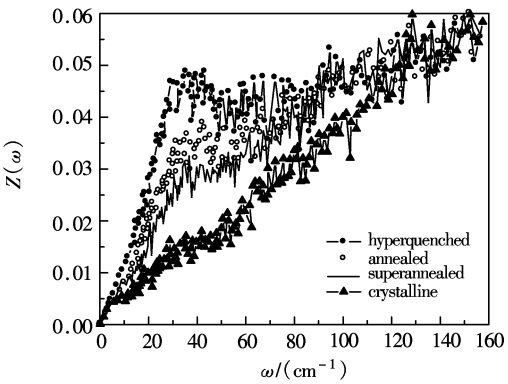

Fig.15　The $Z(\omega)$ function [9] up to 160 cm^{-1} for the basaltic glass in hyperquenched, annealed and super-annealed states, and the crystal state of the basaltic system (composition described in the experimental section). ω is the frequency of vibration. Filled circles: HQG sample; Open circles: 'annealed' glass, which should approximate SG regarding the potential energy; Solid line: 'super-annealed' glass obtained by annealing the sample for 21 h at 894 K, i.e., 5.9% below T_g. Filled triangles: crystallized glass obtained by holding the glass at 1 156 K for 150 min. The figure is re-plotted from [9].

By comparing the studies reported in [63-66], the results shown in **Figure 15** suggest that there is a distinct configurational excitation that involves structures in which low frequency modes, presumably with transverse character, are generated[9]. The simplest description of this source of BP would be that of 'resonance modes' that accompany defects with the character of interstitials in crystals[67]. This has been the suggestion of Granato[68] in advancing his interstitialcy theory of liquids. While Granato's description seems too simple to satisfy the requirements of liquid theory, some topologically diverse form of interstitial excitation may eventually prove adequate to describe the observed phenomena.

Indeed, neutron scattering experiments provide information on the vibrational properties of a system confined to a given basin, and particularly on how that vibrational structure changes with state of configurational excitation of liquid. Since successful computer simulation studies of silicate glass systems have been made by a number of workers[69-70], it is reasonable to hope that studies of inherent structure densities of states, in systems of different

compositions, might help clarify what sort of modes are involved. A detailed discussion about the BP of the HQG subjected to different degrees of annealing is given in [9-11].

To further explore the origin of the enhancement of the VDOS of glasses at low frequencies by increasing T_f, the vibrational properties of a hyperquenched and an annealed glass have been measured using nuclear inelastic scattering [10]. **Figures 16(a)** shows the reduced density of states for both as-produced and annealed HQSilicate in absolute units. The hyperquenched sample shows a higher number of vibrational states in the low-energy region than the annealed glass. This reveals, however, lower density and sound velocity and, therefore, smaller Debye energy. **Figures 16(b)** shows the reduced density of states for both glasses after rescaling the energy axes in Debye energy units and renormalization of the DOS area. It is seen that the VDOS of both samples becomes identical. Thus, the effect of quenching is described by the transformation of the continuous medium. The details of the evaluation are given elsewhere[10].

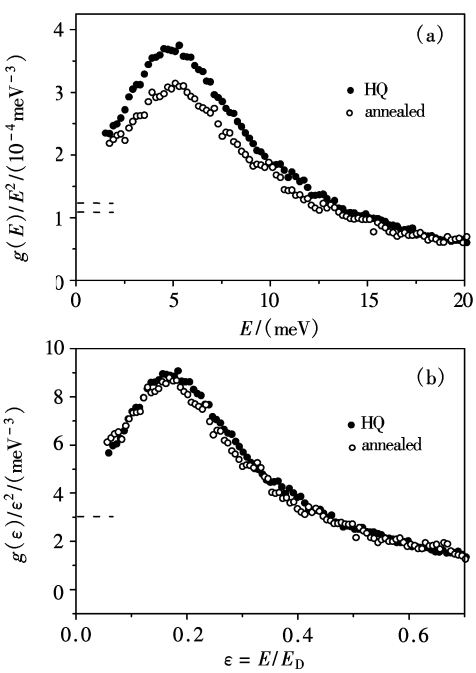

Fig.16 (a) Vibrational density of states (VDOS) in absolute units for the hyperquenched iron-containing soda lime silicate glass (for short, HQSilicate glass) and the annealed HQ-Silicate glass; (b) Reduced VDOS after rescaling the energy axes in Debye energy units and renormalization of the DOS area. The open and solid circles show the data for the hyperquenched and the annealed sample, respectively. The horizontal dashed lines at $E = 0$ show the calculated Debye level. The figure is re-plotted from [10]

In particular, this implies that quenching does not affect the height of the boson peak, i.e., the relative excess of states above the Debye level. The increase of the number of states is compensated by a corresponding increase of the Debye level. However, this implication cannot be seen from the neutron scattering results shown above. Therefore, in future it would be important to perform additional neutron scattering experiments, to rescale the energy axis in Debye energy units, and to renormalize the VDOS area, in order to determine whether or not the above-mentioned implication is reasonable.

6.2 VDOS in nanocrystaline alloy

The dynamics of nanocrystalline materials has attracted a lot of scientific interest during the last decade due to the striking differences observed for their atomic vibrations relative to the bulk counterparts. These anomalies are the enhancement of their density of phonon states (DOS) at low and high energies and broadening of the phonon peaks[71]. Therefore the thorough understanding of the atomic dynamics in these materials is of significant importance not only for fundamental physics, but also for tailoring of their beneficial properties like enhanced strength and hardness, and improved plasticity compared to the coarse-grained materials.

In order to investigate the vibrational dynamics of the nanograins and interfaces systematically, a nanocrystalline $Fe_{90}Zr_7B_3$ alloy prepared by crystallisation of an amorphous precursor has been studied[11]. A ribbon with composition $Fe_{90}Zr_7B_3$ enriched to 63% in ^{57}Fe was produced by the melt-spinning technique. Several nanocrystalline samples composed of α-Fe nanograins and homogeneous and porosity-free interfaces were prepared by annealing of the as-quenched ribbon in a vacuum of 1.6×10^{-6} mbar. **Figure 17** shows a comparison in VDOS between the interfaces (see solid circles), and nanograins (see open circles) for the nano-crystalline $Fe_{90}Zr_7B_3$ materials (see the inset), and between nano-grains and bulk α-Fe (see the dashed line). In the figure, it can be seen that the VDOS of the interfaces is significantly enhanced below 20 meV and slightly above 38 meV in comparison to those of both the nanograins and the bulk α-Fe, whereas the VDOS of nanograins is very close to that of the bulk α-Fe. In [11] it is also proved that the enhancement of the VDOS at low and high energies becomes pronounced with decreasing the degree of heat treatment, and hence, increasing the thickness of the amorphous interfaces, and finally the peaks at 27 and 36 meV vanish (see also **Figure 17**). The DOS of

the nanograins does not vary with their size and down to 2 nm grains still closely resembles that of the bulk. All these results imply that the vibrational anomalies of the nanocrystalline materials, i.e., the enhancement of the VDOS at low and high energies with the continuous decrease of the grain size of nanocrystals, do not originate from the nanograins but from the interfaces. This means that the 'size effect' often found in nanomaterials does not apply to their vibrational properties (VDOS). In order to estimate a proximity of the vibrational properties of the grains to the bulk iron, the DOS of the nanograins was compared to the α-Fe DOS convoluted with the damped harmonic oscillator function.

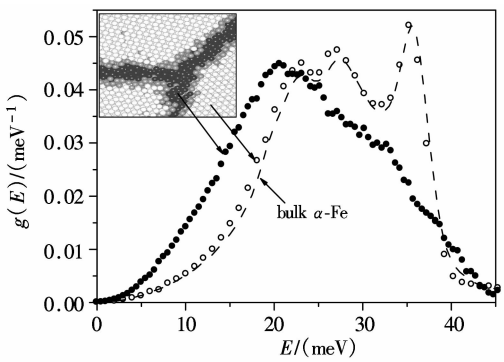

Fig. 17　VDOS of the interfaces (solid circles) and of nanograins (open circles) for the nano-crystalline $Fe_{90}Zr_7B_3$ materials. Dashed line: the VDOS of bulk α-Fe convoluted with the damped harmonic oscillator function with a quality factor $Q = 36$. Inset: schematic representation of both the nano-interfaces and nano-grains, respectively. The figure is re-plotted from [11].

The large suppression of the excessive VDOS at low and high energies as a result of the decrease of interface layers in nanocrystalline alloy suggests that in such thin interface layers (about 2 atomic layers thick) the atoms follow the vibrations of the neighbouring nanograins.

6.3 Perspectives

The studies on the VDOS in nano-crystalline alloys have demonstrated the possibility of determining the vibrational entropy S_v of the interface glass phase[11]. Recently, from VDOS measurements, Gjersing et al succeeded in determining the S_v of a chalcogenide glass and supercooled liquid as a function of T[72]. Determination of S_v is crucial for obtaining a reasonable T dependence of configurational entropy (S_c) of a glass above T_g. This is because S_c can be obtained simply by subtracting the S_v from the total excess entropy (ΔS_{exc}) of a HQG relative to that of its corresponding crystal.

According to Adam-Gibbs (AG) theory, the dynamics and thermodynamics of glass-forming liquids are coupled through S_c that is inversely proportional to the size of the cooperatively rearranging regions. In spite of its beauty and plausibility, the AG model also encounters problems when it is applied to describe the T dependence of relaxation time. This is because S_c cannot be directly measured, and a precise, real temperature dependence of S_c cannot be derived. Instead, the AG theory simply assumes that the excess entropy (ΔS_{exc}) of a liquid relative to its counterpart glass at T_g is close to S_c, and hence, it can be used as S_c. According to the AG theory, ΔS_{exc} equals $\Delta C_p \ln T/T_k$, where T_k is the Kauzmann temperature and ΔC_p is the difference between the liquid and the glass C_p at T_g, which is constant over T. Most of the S_c values reported in literature are actually the ΔS_{exc} values obtained using the calorimetric method. In reality, ΔS_{exc} contains both S_c and S_v, both of which are coupled through their T dependence. In the recent years, different approaches have been used to separate ΔS_c from ΔS_{exc}[73], but the results are often conflicting. On the other hand, a promising effort has been made in determination of S_c. First, scientists are now able to accurately determine ΔS_v from the low frequency VDOS by means of various spectroscopic scattering methods[11,72]. Second, it is possible to precisely determine ΔS_{exc} using the calorimetric method. Thus, ΔS_c is obtained by subtracting ΔS_v from ΔS_{exc}. Moreover, it is possible to make glasses with various T_f values by varying quenching rate and varying the annealing time, and to obtain ΔS_v values of these glasses from the VDOS data, so that the T dependence of S_c may be obtained. In this way, it will be known how ΔS_c is coupled with ΔS_v. Only when the real $\Delta S_c(T)$ function is found, a general picture about the correlation between dynamics and thermodynamics can be established.

7　Concluding remarks

The HAC approach is a powerful tool, by which the enthalpy relaxation in glasses, and dynamics and thermodynamics of supercooled liquids can be probed. The HAC experiments provide information on the energy that can be trapped in glasses by hyperquenching, relative to the

'standard' glass, and on the magnitude of barriers separating basins of attraction on the landscape. The simple methods for determining the fictive temperature and the cooling rate have been established based on the isobaric heat capacity and viscosity measurements. Numerous striking features of the annealing-induced pre-endotherm, e.g. its reversibility and sensitivity to the annealing conditions, are discovered, and thereby, the glass transition of water has been clarified to some extent despite the remaining problems with a precise reassignment of the water T_g. Probably, a direct determination of the water T_g will never be done due to the strong tendency of glassy water to crystallize. Stepwise annealing studies also give information on the matter of energy heterogeneity and the question of 'nanogranularity' in liquids near T_g. The HAC experiments lead to the findings of the Johari-Goldstein (JG) relaxation both in the strong glass GeO_2 and in a metallic glass former. This implies that the JG feature might be a universal feature for all kinds of glass formers. The striking difference in relaxation behaviour between the strong and the fragile glass formers reveals the difference in their energy landscape and structural heterogeneities. A new stretching composite relaxation function describing the non-exponentiality and two relaxation time distributions has been proposed, which successfully describes the C_p curves of the fragile HQGs with different annealing degrees.

The neutron and the inelastic nuclear scattering experiments give information on the vibrational properties of a system confined to a given basin, and particularly on how that vibrational structure changes with the state of configurational excitation of the liquid. An enhancement of the low energy VDOS both in HQGs and in nanocrystalline metallic materials, relative to the 'standard' glass, has been demonstrated. It reveals, however, lower density and sound velocity and, therefore, less Debye energy. After rescaling the energy axes in Debye energy units and area renormalization, the density of states of both samples becomes identical. Thus, the effect of quenching is described by the transformation of the continuous medium. Furthermore, it is found that, for the nanocrystalline materials, the enhancement of the VDOS at low and high energies with the continuous decrease of the grain size of nanocrystals does not originate from the nanograins but from the interfaces.

For continuous HQG fibers, both the anisotropic structural relaxation and the enthalpy relaxation simultaneously occur during annealing, but the former is faster than the latter. This observation implies that the anisotropic structural relaxation results from fast relaxation of the local structure, while the enthalpy relaxation results from slow relaxation of larger domains of the network.

Acknowledgements

The author thanks C. A. Angell, T. Knudsen, S. L. Jensen, M. Guldberg, M. Solvang, R. von der Ohe, E. R. Nielsen, D. Lybye, E. Mollerup, L. Hornbøll, L. N. Hu, M. Ya, N. Lonnroth, M. Lund, S. Stankov, A. Monaco, A. I. Chumakov, J. Deubener, X. F. Bian, and all my present co-workers for useful discussions and collaborations.

References:

[1] ANGELL C A. Formation of glasses from liquids and biopolymers [J]. Science, 1995, 267(5206):1924-1935.

[2] JENSEN M, KEDING R, HÖCHE T, et al. Biologically formed mesoporous amorphous silica[J]. Journal of the American Chemical Society, 2009, 131(7):2717-2721.

[3] ANDERSON P W. Through the glass lightly[J]. Science, 1995, 267(5204):1616-1618.

[4] ANGELL C A, NGAI K L, MCKENNA G B, et al. Relaxation in glass-forming liquids and amorphous solids[J]. Journal of Applied Physics, 2000, 88(6):3113-3157.

[5] ANGELL C A. Insights into phases of liquid water from study of its unusual glass-forming properties[J]. Science, 2008, 319 (5863):582-587.

[6] YUE Y Z, JENSEN S L, CHRISTIANSEN J. Physical aging in a hyperquenched glass[J]. Applied Physics Letters, 2002, 81 (16):2983-2985.

[7] YUE Y Z, ANGELL C A. Clarifying the glass-transition behavior of water by comparison with hyperquenched inorganic glasses [J]. Nature, 2004, 427(6976):717-720.

[8] YUE Y Z, ANGELL C A. Water behavior[J]. Nature, 2005, 435(7041):E1-E2.

[9] ANGELL C A, YUE Y Z, WANG L M, et al. Potential energy, relaxation, vibrational dynamics and the boson peak, of hyperquenched glasses[J]. Journal of Physcis: Condensed Matter, 2003, 15(11):S1051-S1068.

[10] MONACO A, CHUMAKOV A I, YUE Y Z, et al. Density of vibrational states of a hyperquenched glass[J]. Physical Review Letters, 2006, 96(20):205502.

[11] STANKOV S, YUE Y Z, MIGLIERINI M, et al. Vibrational properties of nanograins and interfaces in nanocrystalline materials[J]. Physical Review Letters, 2008, 100(23):235503

[12] (a) HU L N, YUE Y Z. Secondary relaxation behavior in a strong glass[J]. Journal of Physical Chemistry B, 2008, 112 (30):9053-9057.

(b) HU L N, YUE Y Z. Secondary relaxation in metallic glass formers: its correlation with the genuine Johari-Goldstein relaxation [J]. Journal of Physical Chemistry C, 2009, 113(33): 15001-15006.

[13] YUE Y Z. Fragility of a calcium phosphate melt and relaxation of its glass fibers[J]. Phosphorus Research Bulletin, 2002, 13: 39-50.

[14] HORNBOLL L, YUE Y Z. Enthalpy relaxation in hyperquenched glasses of different fragility[J]. Journal of Non-Crystalline Solids, 2008, 354(17): 1862-1870.

[15] YUE Y Z, CHRISTIANSEN J D, JENSEN S L. Determination of the fictive temperature for a hyperquenched glass[J]. Chemical Physics Letters 357(2002) 20-24.

[16] YUE Y Z, von der Ohe R, JENSEN S L. Fictive temperature, cooling rate and viscosity of glasses[J]. Journal of Chemical Physics, 2004, 120(17): 8053-8059; 2004, 121(22): 11508.

[17] RUFFER R, CHUMAKOV A I. Nuclear resonance beamline at ESRF[J]. Hyperfine Interactions, 1996, 97-8(1-4): 589-604.

[18] CHUMAKOV AI, STURHAHN W. Experimental aspects of inelastic nuclear resonance scattering[J]. Hyperfine Interactions, 1999, 123(1-8): 781-808.

[19] YUE Y Z, KORSGAARD M, KIRKEGAARD L F, et al. Formation of a nanocrystalline layer on the surface of stone wool fibers, Journal of the American Ceramic Society, 2009, 92(1): 62-67.

[20] ANGELL C A, WANG LM, MOSSA S, et al. Vibrational dynamics and thermodynamics, ideal glass transitions and folding transitions, in liquids and biopolymers[C]. AIP Conference Proceedings, [s.n.]: [S.l.] 2004, 708: 473-482.

[21] AVRAMOV I, MILCHEV A. Effect of disorder on diffusion and viscosity in condensed systems[J]. Journal of Non-Crystalline Solids, 1988, 104(2-3): 253-260.

[22] YUE Y Z. Characteristic temperatures of enthalpy relaxation in glass[J]. Journal of Non-Crystalline Solids, 2008, 354(12-13): 1112-1118.

[23] YUE Y Z. The iso-structural viscosity, configurational entropy and fragility of oxide liquids[J]. Journal of Non-Crystalline Solids, 2009, 355(10-12): 737-744.

[24] MOYNIHAN CT. Structural relaxation and the glass transition [J]. Review in Mineralogy, 1995, 32: 1-19.

[25] HODGE I M. Enthalpy recovery in amorphous materials[J]. Journal of Non-Crystalline Solids, 1994, 169(3): 211-266.

[26] HUANG J, GUPTA P. Enthalpy relaxation in thin glass fibers [J]. Journal of Non-Crystalline Solids, 1992, 151(1-2): 175-181.

[27] INOUE A, MASUMOTO T, CHEN H S. Enthalpy relaxation behaviour of metal-metal(Zr-Cu) amorphous alloys upon annealing[J]. Journal of Materials Science, 1985, 20: 4057-4068.

[28] WANG L M, BORICK S, ANGELL C A. An electrospray technique for hyperquenched glass calorimetry studies: Propylene glycol and di-n-butyl phthalate[J]. Journal of Non-Crystalline Solids, 2007, 353(41-43): 3829-3837.

[29] GIOVAMBATTISTA N, ANGELL C A, SCIORTINO F, et al. Glass-transition temperature of water: a simulation study[J]. Physical Review Letters, 2004, 93(4): 047801.

[30] MAURO J C, LOUCKS R J. Impact of fragility on enthalpy relaxation in glass[J]. Physical Review E, 2008, 78(2): 021502.

[31] DEBENEDETTI P G, STILLINGER F H. Supercooled liquids and the glass transition[J]. Nature, 2001, 410(6825): 259-267.

[32] YUE Y Z. Influence of physical ageing on the excessive heat capacity of hyperquenched silicate glass fibres[J]. Journal of Non-Crystalline Solids, 2004, 348: 72-77.

[33] YUE Y Z. Calorimetric studies of the structural heterogeneity of silicate liquids[J]. Ceramic Transaction, 2004, 170: 31-45.

[34] YUE Y Z. Features of the relaxation in hyperquenched inorganic glasses during annealing[J]. Physics and Chemistry of Glasses, 2005, 46: 354-358.

[35] HORNBOLL L, YUE Y Z. Enthalpy relaxation of hyperquenched glasses and its possible link to α and β-relaxations [J]. Journal of Non-Crystalline Solids, 2008, 354(2-9): 350-354.

[36] MORENO A J, BULDYREV S V, La Nave E, et al. Energy landscape of a simple model for strong liquids[J]. Physical Review Letters, 2005, 95(15): 157802.

[37] YA M, DEUBENER J, YUE Y Z. Enthalpy and anisotropy relaxation of glass fibers[J]. Journal of the American Ceramic Society, 2008, 91(3): 745-752.

[38] DEUBENER J, YUE Y Z, BORNHOFT H, et al. Decoupling between birefringence decay, enthalpy relaxation and viscous flow in calcium boroalumosilicate glasses[J]. Chemical Geology, 2008, 256(3-4): 299-305.

[39] JENNISKENS P, BANHAM S F, BLAKE D F, et al. Liquid water in the domain of cubic crystalline ice I-c[J]. Journal of Chemical Physics, 1997, 107: 1232-1241.

[40] PRYDE J A, JONES G O. Properties of vitreous water[J]. Nature, 1952, 170: 635-639.

[41] ANGELL C A. Liquid fragility and the glass transition in water and aqueous solutions[J]. Chemical Review, 2002, 102: 2627-2649.

[42] JOHARI G P, HALLBRUCKER A, MAYER E. The glass transition of hyperquenched glassy water[J]. Nature, 1987, 330: 552-553.

[43] HALLBRUCKER A, MAYER E, JOHARI G P. Glass-liquid transition and the enthalpy of devitrification of annealed vapor-deposited amorphous solid water. A comparison with hyperquenched glassy water[J]. Journal of Physical Chemistry, 1989, 93: 4986-4990.

[44] MACFARLANE D R, ANGELL C A. Nonexistent glass transition for amorphous solid water[J]. Journal of Physical Chemistry, 1984, 88:759-762.

[45] VELIKOV V, BORICK S, ANGELL C A. The glass transition of water, based on hyperquenching experiments[J]. Science, 2001, 294(5550):2335-2338.

[46] JOHARI G P. Does water need a new Tg? [J]. Journal of Chemical Physics, 2002, 116:8067-8073.

[47] ANGELL C A. Amorphous water[J]. Annual Review of Physical Chemistry, 2004, 55:559-583.

[48] ANGELL C A. Insights into phases of liquid water from study of its unusual glass-forming properties[J]. Science, 2008, 319 (5863):582-587.

[49] KOHL I, BACHMANN L, MAYER E, et al. Water behaviour-glass transition in hyperquenched water? [J]. Nature, 2005, 435(7041):E1-E1.

[50] SETTE F, KRISCH M H, MASCIOVECCHIO C, et al. Dynamics of glasses and glass-forming liquids studied by inelastic X-ray scattering[J]. Science, 1998, 280(5369):1550-1555.

[51] BUCHENAU U, PRAGER M, NUCKER N, et al. Low-frequency modes in vitreous silica[J]. Physical Review B, 1986, 34(8):5665-5673.

[52] BUCHENAU U, ZHOU H M, NUCKER N, et al. Structural relaxation in viteous silica[J]. Physical Review Letters, 1988, 60(13):1318-1321.

[53] SOKOLOV A P, BUCHENAU U, STEFFEN W, et al. Comparison of Raman- and neutron-scattering data for glass-forming systems[J]. Physical Review B, 1995, 52(14):R9815-R9818.

[54] ELLIOTT S R. A unified model for the low-energy vibrational behavior of a morphous solids[J]. Europhysics Letters, 1992, 19(3):201-206.

[55] DUVAL E, BOUKENTER A, CHAMPAGNON B. Vibration eigenmodes andsize of microcrystallites in glass-observation by very-low-frequency Raman-scattering[J]. Physical Review Letters, 1986, 56(19):2052-2055.

[56] DOVE M T, HARRIS M J, HANNON A C, et al. Floppy modes in crystalline and amorphous silicates[J]. Physical Review Letters, 1997, 78(6):1070-1073.

[57] NAKAMURA M, ARAI M, INAMURA Y, et al. Effect of low-energy dynamics on anomalous vibrational amplitudes in vitreous silica[J]. Phys Rev B, 2002, 66(2):024203.

[58] COURTENS E, FORET M, HEHLEN B, et al. The vibrational modes of glasses[J]. Solid State Communications, 2001, 117 (3):187-200.

[59] GREAVES G N, MENEAU F, MAJERUS O, et al. Identifying vibrations that destabilize crystals and characterize the glassy state[J]. Science, 2005, 308(5726):1299-1302.

[60] HOLOMB R, MITSA V. Boson peak of As_xS_{1-x} glasses and theoretical calculations of low frequencies clusters vibrations [J]. Solid State Communications, 2004, 129(10):655-659.

[61] PHILLIPS J C. Topology of covalent non-crystalline solids .2. Medium-range order in chalcogenide alloy and a-Si(Ge)[J]. Journal of Non-Crystalline Solids, 1981, 43(1):37-77.

[62] LUCOVSKY G, WONG C K, POLLARD W B. Vibrational properties of glasses: intermediate range order[J]. Journal of Non-Crystalline Solids, 1983, 59-60:839-846.

[63] PHILLIPS W A, BUCHENAU U, NUCKER N, et al. Dynamics of glassy and liquid selenium[J]. Physical Review Letters, 1989, 63(21):2381-2384.

[64] SUCK J B. Low energy dynamics in glasses investigated by neutron inelastic scattering[J]. Advances in Solid State Physics, 2002, 42:393-403.

[65] SUCK J B. Dynamics of amorphous materials[C]. Springer Proc Phys, Heidelberg:Springer, 1989:182.

[66] VOLLMAYR k, KOB w, BINDER k. Cooling-rate effects in amorphous silica:a computer-simulation study[J]. Physical Review B, 1996, 54(22):15808-15827.

[67] DEDERICHS P H, LEHMAN C, SCHOBER H R. et al. Lattice theory of point defects[J]. Journal of Nuclear Materials, 1978, 69-70(1-2):176-199.

[68] GRANATO A V. Interstitialcy model for condensed matter states of face-centered-cubic metals[J]. Physical Review Letters, 1992, 68(7):974-977.

[69] VESSAL B, GREAVES G N, MARTEN P T, et al. Cation microsegregation and ionic mobility in mixed alkali glasses[J]. Nature, 1992, 356(6369):504-506.

[70] HORBACH J, KOB W. The structural relaxation of molten sodium disilicate[J]. Journal of Physics: Condensed Matter, 2002, 14(40):9237-9253.

[71] SURYANARAYANA C, KOCH C C. Nanocrystalline materials-current research and future directions[J]. Hyperfine Interactions 2000, 130(1-4):5-44.

[72] GJERSING E L, SEN S, AITKEN B G. Vibrational entropy near glass transition in a chalcogenide glass and supercooled liquid[J]. Journal of Non-Crystalline Solids, 2009, 355(10-12):748-752.

[73] JOHARI G P. Decrease in the configurational and vibrational entropies on supercooling a liquid and their relations with the excess entropy[J]. Journal of Non-Crystalline Solids, 2002, 307:387-392.

(编辑:胡春霞)